JOURNAL OF PROPULSION AND POWER
Vol. 19, No. 4, July–August 2003

One-Dimensional Hollow Cathode Model

Ira Katz,* John R. Anderson,† James E. Polk,‡ and John R. Brophy‡
Jet Propulsion Laboratory, California Institute of Technology, Pasadena, California 91109

Hollow cathodes with barium-rich inserts are used in ion engines as electron sources both in the discharge chamber and to neutralize the ion beam. Future deep space missions will require hollow cathode lifetimes in excess of the 28,000 h demonstrated during the International Space Station plasma contactor hollow cathode life test. A hollow cathode model is developed based on the observation that xenon ion mobility is diffusion limited due to resonant charge exchange reactions. Application of the model to the orifice region shows that the resultant ion generation profile correlates with previously reported orifice erosion. Modeling of the insert region shows that vapor-phase barium atoms are ionized almost immediately and electric fields accelerate the ions upstream from the "emission zone."

Nomenclature

C	=	eigenvalue associated with Bessel function
D_a, D_e, D_i	=	ambipolar, electron, and ion diffusion rates, $m^2 \cdot s^{-1}$
E_i	=	xenon first ionization energy, 12.1 eV
E_z	=	axial electric field strength, $V \cdot m^{-1}$
e	=	electron charge, 1.60×10^{-19} C
f	=	fraction of neutrals with ion radial speed
I_e	=	electron current, A
$J_0(), J_1()$	=	zero-order and first-order Bessel functions
j_e	=	electron current density, $A \cdot m^{-2}$
k	=	Boltzman constant, 1.38×10^{-23} JK^{-1}
M	=	xenon mass, 2.20×10^{-25} kg
m_e	=	electron mass, 9.11×10^{-31} kg
n	=	plasma number density, m^{-3}
n_e, n_i, n_0	=	electron, ion, and neutral number densities, m^{-3}
$n(0)$	=	ion number density at centerline, m^{-3}
$\dot{n}$	=	plasma production rate, $m^{-3} \cdot s^{-1}$
$\bar{n}$	=	radially averaged ion number density, m^{-3}
P	=	xenon pressure, Pa
R	=	orifice radius, m
r	=	radial coordinate, m
T	=	neutral xenon temperature, K
T_e, T_i	=	electron, and ion temperature, eV
T_r	=	reduced temperature, K
T_{wall}	=	orifice wall temperature, K
u_e, u_i	=	electron and ion axial velocities, $m \cdot s^{-1}$
u_r	=	ion radial velocity, $m \cdot s^{-1}$
u_{scat}	=	ion scattering speed, $m \cdot s^{-1}$
u_{th}	=	ion thermal speed, $m \cdot s^{-1}$
u_{wall}	=	ion velocity to orifice wall, $m \cdot s^{-1}$
u_0	=	neutral axial velocity, $m \cdot s^{-1}$
z	=	axial coordinate, m
ε_0	=	permittivity of free space, 8.85×10^{-12} $C \cdot V^{-1} \cdot m^{-1}$
ζ	=	viscosity, $Pa \cdot s$
η	=	plasma resistivity, $V \cdot m \cdot A^{-1}$
κ	=	electron thermal conductivity, A/m
Λ	=	Coulomb log
λ_{01}	=	first zero of zero-order Bessel function, 2.405
μ_e, μ_i	=	electron and ion mobility, $m^2 \cdot V^{-1}$ s^{-1}
π	=	ratio of circumference to diameter of a circle
σ_{CEX}	=	charge exchange cross section, m^2
$\sigma_{\text{en}}(T_e)$	=	Maxwellian averaged electron–neutral collision cross section, m^2
$\sigma(T_e)$	=	Maxwellian averaged ionization cross section, m^2
τ_{CEX}	=	average time between charge exchange collisions for a xenon particle, s
τ_e	=	average time between electron collisions, s
τ_i	=	average time between ion collisions, s
τ_{wall}	=	average time between collisions with wall for a xenon particle, s
υ_{ei}	=	electron–ion collision frequency, s^{-1}
υ_{en}	=	electron–neutral collision frequency, s^{-1}
ω_p	=	plasma frequency, s^{-1}

Received 14 August 2002; revision received 28 February 2003; accepted for publication 3 March 2003.

*Supervisor, Advanced Propulsion Technology Group, MS 125-109, 4800 Oak Grove Drive; ira.katz@jpl.nasa.gov. Senior Member AIAA.

†Senior Engineer, Advanced Propulsion Technology Group, MS 125-109, 4800 Oak Grove Drive. Senior Member AIAA.

‡Principal Engineer, Advanced Propulsion Technology Group, MS 125-109, 4800 Oak Grove Drive. Senior Member AIAA.

Introduction

HOLLOW cathodes are a critical component of most electrostatic and Hall effect ion thrusters. The record life of a hollow cathode was for the International Space Station plasma contactor test run at NASA John H. Glenn Research Center at Lewis Field.[1] During this test, the hollow cathode performance changed after 23,000 h of operation, and the cathode finally failed to restart after 28,000 h, or just over 3 years. This endurance is impressive and exceeds present demands on a hollow cathode for solar electric propulsion missions. However, on missions to the outer planets, electric thrusters will be required to operate for more than 5 years.[2] Because of this need, we have begun a systematic investigation to model the processes that can cause hollow cathode performance degradation and failure.

In a hollow cathode, electrons transfer between neutral gas atoms and ionized propellant through resonant charge exchange (CEX). The CEX cross section between Xe and Xe^+ is so large at low ion energies and the densities are so high that inside hollow cathodes, ion mobility is diffusion limited. When literature values for the cross section[3] are used, at a cathode pressure of 10 torr, the ion mean free path for resonant CEX is less than 5×10^{-6} m, much less than cathode orifice dimensions. The model to be described builds on the limited ion mobility to construct a set of fluid equations that describe the cathode plasma. A straightforward application of the model leads to a new description of hollow cathode processes.

In the orifice region, we have a new one-dimensional, variable cross section model that extends the previous model of Katz et al.[4] to include CEX collisions, a radial density profile, axial variation in all parameters, and neutral gas viscosity. The model shows that the axial variation of ion currents bombarding the orifice walls is in agreement with published shapes of neutralizer orifice erosion.[5]

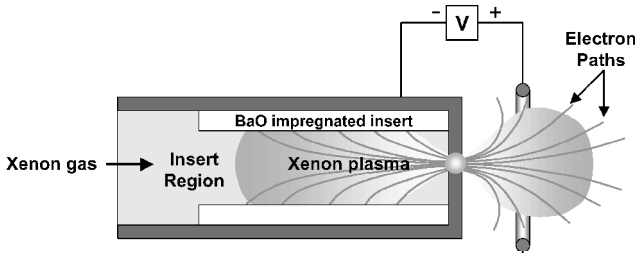

Fig. 1 Schematic of hollow cathode operation.

In the insert region, the electron temperature from this model agrees well with published spectroscopic measurements[6] and langmuir probe measurements (see Ref. 7). The model shows that vapor-phase barium atoms are quickly ionized. When the electron impact ionization cross section[8,9] is integrated over a thermal distribution, barium atoms are ionized in less than a microsecond in the insert region plasma, that is, much less than the atom transit time across the insert. Plasma electric fields transport barium ions upstream. This is in contrast with previous work[10] that only included neutral barium diffusion and convection downstream by neutral xenon gas. The effective velocities of barium ions are in the opposite direction of the barium neutral model reported previously.

Background

A hollow cathode consists of a metal tube lined with a sintered tungsten insert capped at one end by a plate with a small orifice, as shown in Fig. 1. Electrons are emitted from the barium oxide, calcium oxide, aluminate impregnated insert. Propellant gas, typically xenon, flows into the tube and exits, partially ionized, out of the orifice. Electrons flow from the insert region, through the orifice plasma to keeper and other anode surfaces. Whereas most of the electrons emanate from the insert material, one of the results in this paper is to show that electrons are generated by ionization of the propellant gas and the circuit completed by ions impacting the inner walls of the orifice. Calculations for NASA's Solar Electric Propulsion Technology Application Readiness (NSTAR) ion thruster neutralizer design[11] operating at full power show that one-third of the electrons are generated by ionization in the orifice.

The model presented builds on a previously published model of orifice processes that ignored axial variation; instead, it treated "the orifice as a cylinder containing a homogeneous neutral plasma."[4] The previous zero-dimensional model also assumed that the ion loss rate to the walls was the product of the wall area and the ion thermal flux, assuming the ions had a Maxwellian velocity distribution with the electron temperature. This simplifying assumption is removed in the present work, where the ion motion is determined from the ambipolar diffusion equation. Another approximation eliminated in the present model is the use of a temperature-independent electron–neutral elastic cross section. The earlier model included power loss due to radiation; however, radiation is neglected in the present model because the plasma is optically thick and most of the radiation is trapped inside the plasma.[6]

Orifice Plasma Model

Inside the orifice, the electron current density is the highest, and classical electron scattering leads to resistive heating. These hot electrons ionize a fraction of the xenon gas, and although most of the ions hit the walls of the orifice, some escape downstream. These ions provide charge neutralization for the electron current exterior to the cathode.

In the model, neutral xenon gas and electrons enter the orifice from the insert region, neutral xenon and electrons exit downstream, and xenon ions exit both upstream and downstream. The computational region includes the orifice and the chamfered expansion region, shown in Fig. 2. Most of the ions that are created in the orifice recombine on the walls, as shown in Fig. 3. We assume that the electrons behave as a classical fluid, that the neutral xenon gas flow is Poiseuille flow, and that the ion flow is diffusion limited because

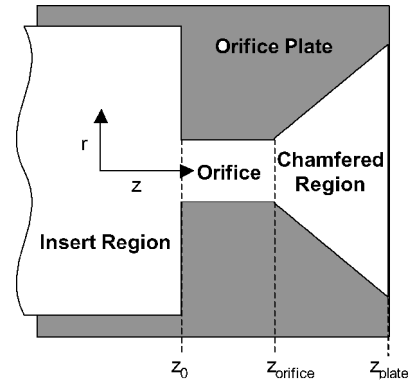

Fig. 2 Volume modeled includes the orifice and the chamfered region.

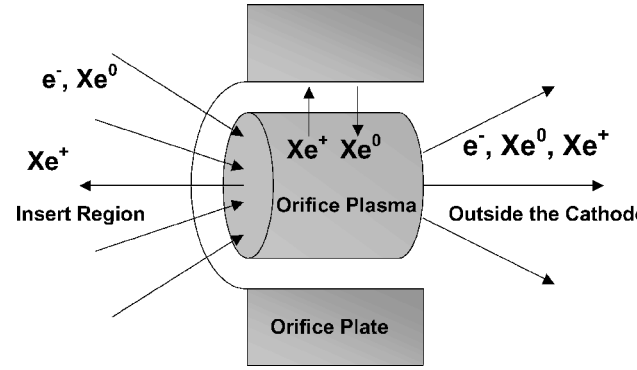

Fig. 3 Most of the ions created in the orifice recombine on the walls.

of the short mean free path, $<5 \times 10^{-6}$ m, for resonant CEX with neutrals. It is the very short ion mean free path for resonant CEX that controls the plasma density radial profile and loss rates.

Mass Continuity Equations

With the assumption of quasi neutrality

$$n = n_i \approx n_e \tag{1}$$

the local ionization rate links the steady-state continuity equations for neutral xenon, xenon ions, and electrons:

$$-\dot{n} + \nabla \cdot u_0 n_0 = 0 \tag{2}$$

$$\dot{n} + \nabla \cdot u_i n = 0 \tag{3}$$

$$e\dot{n} + \nabla \cdot j_e = 0 \tag{4}$$

The electron current density is

$$j_e \equiv -enu_e \tag{5}$$

The ion-generation rate is

$$\dot{n} = 4\sigma(T_e) n_0 n \sqrt{eT_e/2\pi m_e} \tag{6}$$

The impact ionization cross section for xenon averaged over a Maxwellian distribution of electrons at temperature T_e (in electron volts) is[4]

$$\sigma(T_e) \approx 10^{-20}\left[3.97 + (0.643T_e) - \left(0.0368T_e^2\right)\right] \exp(-E_i/T_e) \tag{7}$$

Including the boundary condition that the ion flux to the orifice walls is balanced by the neutral flux off the walls, and integrating over the orifice radius, we obtain the following equations in the axial

dimension z:

$$\pi R^2\left(-\dot{n}+\frac{\partial u_0 n_0}{\partial z}\right)+2\pi R u_{\text{wall}} n=0 \tag{8}$$

$$\pi R^2\left(\dot{n}+\frac{\partial u_i n}{\partial z}\right)-2\pi R u_{\text{wall}} n=0 \tag{9}$$

$$\pi R^2\left(e\dot{n}+\frac{\partial j_e}{\partial z}\right)=0 \tag{10}$$

The electron current is related to the electron current density by

$$I_e=\pi R^2 j_e \tag{11}$$

In the orifice, u_{wall} is chosen to be the average ion radial velocity u_r derived later. In the chamfered region, where the wall radius expands at a 45-deg angle, the losses are lower because the flow is nearly parallel to the walls. (The axial and radial velocities are comparable.) A true assessment of wall losses in the chamfered region requires a two-dimensional code. In the code, the wall losses are computed using the velocity component perpendicular to the wall; if this velocity component is directed away from the surface in the chamfer region, wall losses are set to zero.

The electron continuity equation accounts for the increase in electron current due to ionization. This current is carried to the walls by the ions. Our calculations show that the current from ionization can account for one-third of the current at typical NSTAR neutralizer operating conditions.

The average neutral gas velocity is determined assuming Poiseuille flow:

$$u_0=-\frac{R^2}{8\zeta}\frac{\mathrm{d}P}{\mathrm{d}z} \tag{12}$$

The temperature-dependent xenon viscosity is found using the corresponding states method.[12] For xenon, the viscosity is

$$\zeta=2.3\times10^{-5}T_r^{0.965} \qquad \text{for} \qquad T_r<1$$

$$\zeta=2.3\times10^{-5}T_r^{0.71+0.29/T_r} \qquad \text{for} \qquad T_r>1$$

$$T_r=T/289.7 \tag{13}$$

As discussed later, ions diffuse radially toward the orifice wall. An ion that undergoes a CEX collision becomes a neutral with the same velocity it had when it was an ion. Because of the large of CEX collision cross section, a large fraction of the neutral xenon will suffer CEX collisions and diffuse toward the wall at the ion radial speed. This causes the viscosity to increase and is incorporated into the model as an increase in neutral xenon temperature,

$$T=T_{\text{wall}}+(M/k)\left[(fu_r)^2+u_0^2\right] \tag{14}$$

The fraction of neutrals that have the ion radial velocity is given by

$$f=1-\exp[-(n/n_0)\tau_{\text{wall}}/\tau_{\text{CEX}}] \tag{15}$$

Heating of neutrals by CEX collisions is consistent with experiments where neutral temperatures greater than the orifice wall temperature have been observed.[13]

The upstream neutral density is determined by the requirement that the sum of the steady-state neutral and ion fluxes entering the orifice equal the specified gas flow rate through the hollow cathode.

Ion and Electron Momentum Equations

We assume that inertial terms are negligible in both the ion and electron momentum equations, an assumption supported by the calculations to follow. We also assume that the axial ion current is small compared with the electron current. The electron momentum equation takes the familiar form of a generalized Ohm's law, as does the ion momentum equation,

$$j_e=eD_e\frac{\partial n}{\partial z}+en\mu_e E_z \tag{16}$$

$$n(u_i-u_0)=-D_i\frac{\partial n}{\partial z}+n\,\mu_i\,E_z \tag{17}$$

For electrons and ions, the diffusion coefficients and the mobilities are defined as

$$D_e=\tau_e(eT_e/m_e) \tag{18}$$

$$D_i=\tau_i(eT_i/M) \tag{19}$$

$$\mu_e=\tau_e(e/m_e) \tag{20}$$

$$\mu_i=\tau_i(e/M) \tag{21}$$

When the axial electric field is eliminated, the ion momentum and electron momentum equations can be combined into a single equation,

$$n(u_i-u_0)=-\left(D_i+\frac{\mu_i}{\mu_e}D_e\right)\frac{\partial n}{\partial z}+\frac{\mu_i}{\mu_e}\left(\frac{j_e}{e}\right)$$

$$=-D_a\frac{\partial n}{\partial z}+\frac{\mu_i}{\mu_e}\left(\frac{j_e}{e}\right) \tag{22}$$

Computational results show that the last term is nonnegligible and that the applied electric field drives ions in the orifice upstream into the insert region. Therefore, ions generated in the insert region do not escape from the cathode.

The ion mobility is limited by resonant CEX with neutral xenon. In the orifice the ion mean free path for CEX collisions is several micrometers. The average time between ion collisions (in seconds) is

$$\tau_i=1/\sigma_{\text{CEX}}n_0u_{\text{scat}} \tag{23}$$

Using this, the ambipolar diffusion coefficient is

$$D_a=(1/\sigma_{\text{CEX}}n_0)(e/M)[(T_i+T_e)/u_{\text{scat}}] \tag{24}$$

For relatively slow diffusion, such as in the insert region, the ion scattering speed can be approximated by the ion thermal speed,

$$u_{\text{th}}=\sqrt{eT_i/M} \tag{25}$$

However, in the orifice, the radial drift velocity frequently exceeds the ion thermal speed, and we use

$$u_{\text{scat}}=\sqrt{u_{\text{th}}^2+(u_i-u_0)^2+u_r^2} \tag{26}$$

The average collision time for electrons is given by

$$\tau_e=1/(\upsilon_{\text{ei}}+\upsilon_{\text{en}}) \tag{27}$$

The electron–ion coulomb scattering frequency is[14]

$$\upsilon_{\text{ei}}=2.9\times10^{-12}n\Lambda T_e^{-\frac{3}{2}} \tag{28}$$

where the coulomb logarithm is

$$\Lambda=23-\tfrac{1}{2}\ln\left(10^{-6}n/T_e^3\right) \tag{29}$$

The electron–neutral collision frequency is

$$\upsilon_{\text{en}}=\sigma_{\text{en}}(T_e)n_0\sqrt{eT_e/m_e} \tag{30}$$

A numerical fit to the electron–neutral scattering cross section averaged over a Maxwellian electron distribution is[15]

$$\sigma_{\text{en}}(T_e)\approx6.6\times10^{-19}\left\{(T_e/4-0.1)/\left[1+(T_e/4)^{1.6}\right]\right\} \tag{31}$$

Ion Radial Flow

As shown later, axial ion density gradients in the interior of the orifice are small, and most of the ions produced are lost by diffusion to the walls. Setting the diffusion loss rate equal to the ion production rate yields

$$-\nabla \cdot [D_a \nabla n] = \dot{n} \tag{32}$$

Ignoring the axial density gradients and radial variations in electron temperature and neutral densities, we obtain

$$\frac{\partial^2 n}{\partial r^2} + \frac{1}{r}\frac{\partial n}{\partial r} + C^2 n = 0 \tag{33}$$

where

$$C^2 = n_0 \sigma(T_e)\sqrt{8eT_e/\pi m_e}\Big/ D_a \tag{34}$$

The solution to Eq. (33) is a zero-order Bessel function,

$$n(r) = n(0) J_0(Cr) \tag{35}$$

Assuming that the ion density goes to zero at the wall, the constant becomes

$$C = \lambda_{01}/R \tag{36}$$

This eigenvalue leads to the following equation that determines the electron temperature:

$$(R/\lambda_{01})^2 n_0 \sigma(T_e)\sqrt{8eT_e/\pi m_e} - D_a = 0 \tag{37}$$

The radially averaged ion density is related to the ion density on the centerline by

$$\bar{n} = \int_0^R n(0) J_0\left(\frac{\lambda_{01}}{R} r\right) 2\pi r \, \mathrm{d}r \Big/ \pi R^2 = n(0)\left[\frac{2J_1(\lambda_{01})}{\lambda_{01}}\right] \tag{38}$$

The radial ion flux at the wall is

$$-D_a \frac{\partial n}{\partial r} = n(0) D_a \frac{\lambda_{01}}{R} J_1(\lambda_{01}) = \bar{n} D_a \frac{(\lambda_{01})^2}{2R} \equiv \bar{n} u_r \tag{39}$$

Substituting the ambipolar diffusion coefficient derived using the CEX collision time, the effective radial drift velocity at the wall is

$$u_r = \frac{(\lambda_{01})^2}{2R\sigma_{\mathrm{CEX}} n_0}\frac{e}{M}\left(\frac{T_i + T_e}{u_{\mathrm{scat}}}\right) \tag{40}$$

Energy Equation

The steady-state electron energy equation is

$$0 = -\nabla \cdot \left(-\tfrac{5}{2} j_e T_e - \kappa \nabla T_e\right) + \eta j_e^2 - \dot{n} e E_i \tag{41}$$

where E_i is the ionization energy of xenon, 12.1 eV. The plasma resistivity is

$$\eta = 1\Big/\varepsilon_0 \tau_e \omega_p^2 \tag{42}$$

and the classical electron thermal conductivity is[14]

$$\kappa = 3.2\left(\tau_e n_e^2 T_e \Big/ m_e\right) \tag{43}$$

Following the analysis of Malik et al.,[6] it appears that the orifice plasma is optically thick, and therefore, radiative losses are neglected.

Insert Region Results

In the insert region, the electron current density is small, except in the vicinity of the orifice. If we drop the electron current terms and assume that the plasma is isothermal, we can use the ion radial flow equations to determine the maximum possible temperature. The model yields an electron temperature of 1.1 eV compared with spectroscopic measurements of 1.1 eV reported by Malik et al.[6] For the insert geometry reported by Domonkos et al.,[7] the model gives an electron temperature of 0.6 eV compared to 0.7–0.8 eV temperatures measured with langmuir probes.

We have solved in two dimensions the isothermal ambipolar diffusion equation to obtain a plasma density distribution inside the insert region (Fig. 4). The ion density in the orifice was fixed at 10^{22} m^{-3}, consistent with the results of the orifice calculations discussed in the next section. The plasma density drops rapidly upstream of the orifice. It can be shown analytically that if the radial variation were a zero-order Bessel function the plasma density would decay exponentially from the orifice.

Vapor-phase barium atoms are quickly ionized due to their low, 5.2 eV, ionization potential. Barium ions are accelerated upstream by the potentials in the insert region as shown in Fig. 5; similar potential variations have been measured using langmuir probes in mercury hollow cathodes.[16] Using this insert region electric field and an approximate mobility ratio for barium ions in xenon,[17] we estimate that barium ions diffuse upstream with a velocity on the order of meters per second. Thus, the effective barium pressure above the active insert material is lower than assumed in the previous work,[10] and this explains why the hollow cathode insert lifetimes are consistent with insert life in vacuum devices.[18] This is also consistent with the observation of barium deposits at the upstream end of the insert after long duration tests.[1,5]

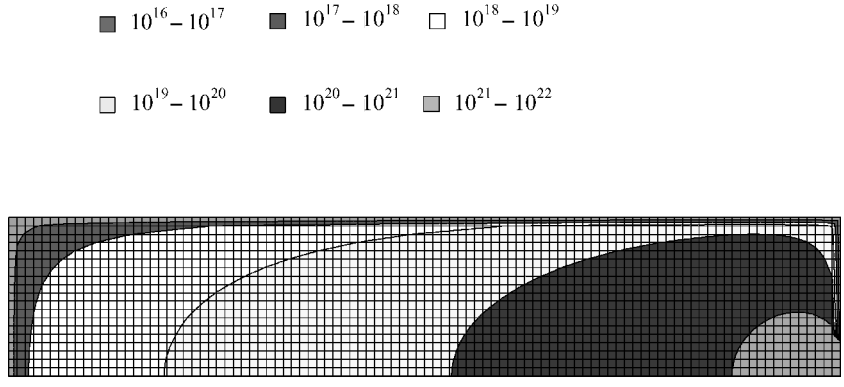

Fig. 4 Plasma number density (per square meter) in the insert region calculated assuming uniform electron temperature.

Orifice Results

We have applied the model to the neutralizer cathode of the NSTAR ion thruster operating at the full power point.[19] At this operating point, the total cathode current is 3.26 A and the xenon gas flow rate is 3.54×10^{-7} kg/s.

Figure 6 shows the computed neutral xenon and ionized xenon number densities in the orifice and chamfer regions. The ion (plasma) density peaks near the center of the orifice and decreases on either side as ions flow out both ends of the orifice. The neutral xenon density decreases as the flow accelerates downstream. The computed upstream pressure for this case is 6.3 kPa (47 torr). We do not have good pressure measurements to compare with this estimate; however, operating pressures in this range have been measured experimentally.[7]

The computed electron temperature, shown in Fig. 7, increases from 1.1 eV in the insert region to about 1.5 eV at the center of the orifice and then rises to about 2 eV as the flow enters the chamfer region.

The calculated electron current through the orifice and chamfer regions is shown in Fig. 8. Most of the ions produced in the orifice diffuse to the wall, while the electrons produced from ionization collisions are extracted downstream. Slightly over 1 A of ion current strikes the orifice wall at the NSTAR full power point. As a result only about two-thirds of the electrons extracted from the neutralizer cathode are supplied from the insert region. Hollow cathode neutralizer orifice erosion has been reported after long duration tests.[1,5] Typically, the greatest enlargement is at the downstream side of the orifice, with the erosion diminishing toward the upstream end. For example, Fig. 9 shows a section through the NSTAR neutralizer hollow cathode orifice plate taken after the 8000-h life test. The cylindrical orifice has been eroded into a conical shape, indicating an axial variation in the orifice environment. This same axial variation in erosion pattern was also reported in the life test of the International Space Station plasma contactor hollow cathode.[1] In the present calculation (Fig. 10), the ion current density at the wall follows a similar profile. Almost all of the ions generated are accelerated radially into the orifice walls. We have not yet included

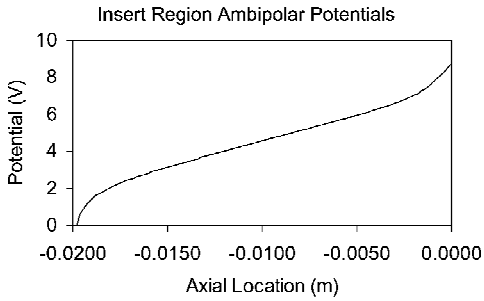

Fig. 5 Potential along the axis in the insert region.

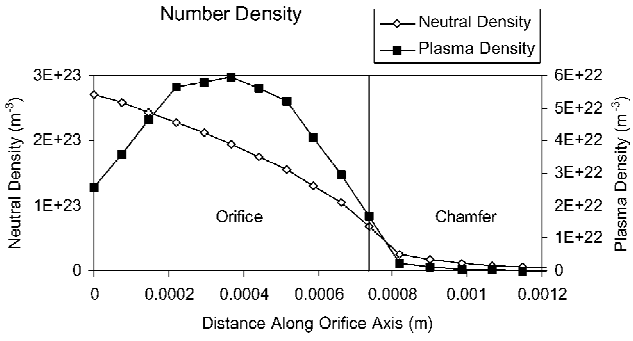

Fig. 6 Calculated neutral and ion densities in the orifice and expansion regions.

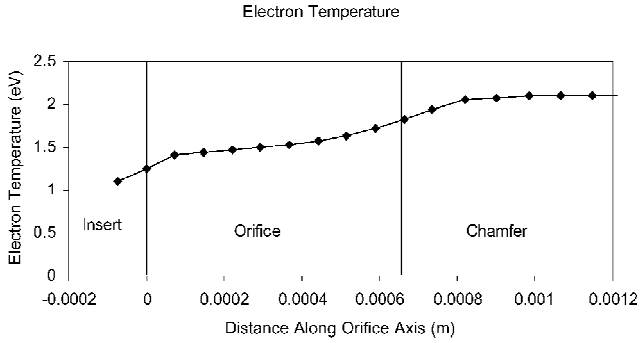

Fig. 7 Calculated electron temperatures in the orifice and expansion regions.

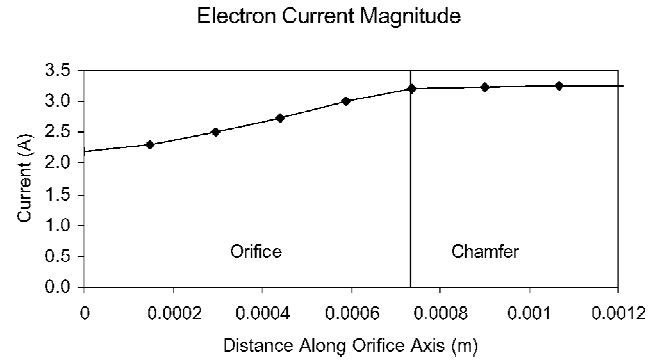

Fig. 8 Calculated electron current in the orifice and expansion regions.

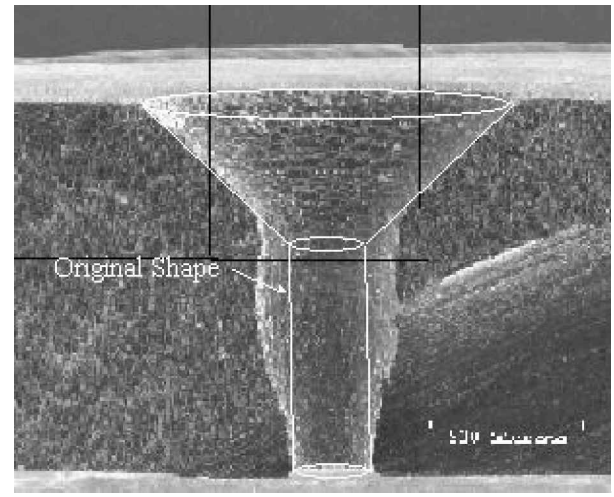

Fig. 9 Neutralizer cathode orifice showing erosion after long duration test.[5]

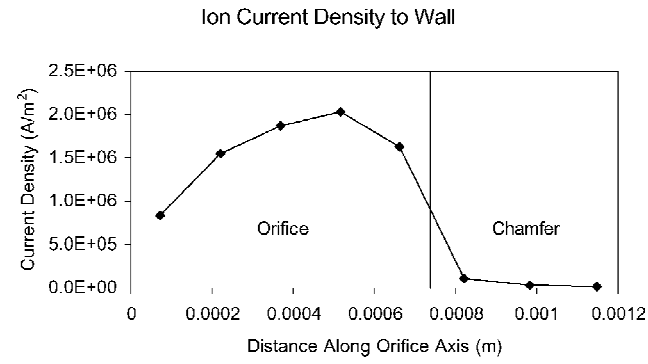

Fig. 10 Calculated initial ion current density along the wall of the uneroded orifice.

double ions or sheath potentials into the model and are, therefore, presently unable to calculate sputtering rates.

The diameter of the NSTAR neutralizer orifice nearly doubled at the downstream end (Fig. 9) during the 8000-h test. Calculations using twice the diameter of the NSTAR neutralizer design show that the current density to the orifice wall decrease by over an order of magnitude. Because the erosion rate is proportional to the current density, the orifice erosion rate is expected to decrease comparably after the diameter doubles. This decrease in current density to the wall occurs because the diffusion rate is lower for larger diameters.

After the 8000-h test, the NSTAR discharge chamber cathode orifice diameter decreased slightly due to deposited material.[5] The discharge chamber cathode orifice diameter is almost four times that of the neutralizer cathode, and over 15 A of electron current was extracted during operation. The model was applied to this cathode, and it predicts that 0.2-A ion current is collected on the orifice wall. The maximum current density at the orifice wall is about 21 times lower than that for the NSTAR neutralizer design, which is consistent with the fact that erosion was not observed.

Summary

We are developing a new model of hollow cathode processes that accounts for the very short propellant ion mean free path for resonant CEX. Our first results, include descriptions of current generation, operating pressure, and ion fluxes to orifice surfaces, as well as a new barium transport model.

In the insert region, the model describes a weakly ionized, quasi-neutral plasma with relatively slow diffusion-limited xenon ion transport. Electron temperatures predicted by the model are in good agreement with recent data. Previous models assumed barium transport was controlled by neutral gas convection. In our model, plasma electric fields drive barium ions with velocities an order of magnitude greater than and in the opposite direction from neutral gas convection.

When applied to the orifice, we found that for small orifice diameters a substantial fraction of the current was generated by ionization of the propellant and subsequent recombination of the ions on the orifice walls. This can result in rapid erosion until the orifice diameter increases enough to result in a significant reduction in propellant ionization in the orifice.

The ions charge exchange with neutrals many times as they are accelerated toward the orifice walls. These multiple CEX collisions act to heat the neutral gas far beyond the orifice plate temperature. This heating increases the gas viscosity, accounting for the pressure rise observed when a hollow cathode discharge is started.[7]

The distribution and magnitude of ionization in the orifice correlates with observed orifice erosion. Additional work in this area, including sheath potentials and double ion generation is needed to allow prediction of orifice erosion rates.

Although the first results are promising, the work presented here is not a complete description of hollow cathode operation. To predict reliably hollow cathode performance and life, additional efforts are required to develop a fully two-dimensional code that includes self-consistent models of insert electron emission, plasma sheaths, multiple ion species, surface temperatures, and radiation.

Acknowledgment

This research was carried out at the Jet Propulsion Laboratory, California Institute of Technology.

References

[1]Sarver-Verhey, T. R., "Destructive Evaluation of a Xenon Hollow Cathode After a 28,000 Hour Life Test," AIAA Paper 98-3482, July 1998.

[2]Noca, M., Frisbee, R., Johnson, L., Kos, L., Gefert, L., and Dudzinski, L., "Evaluating Advanced Propulsion Systems for the Titan Explorer Mission," International Electric Propulsion Conf., IEPC Paper 01-175, Oct. 2001.

[3]Miller, J. S., Pullins, S. H., Levandier, D. J., Chiu Y., and Dressler, R. A., "Xenon Charge Exchange Cross Sections for Electrostatic Thruster Models," *Journal of Applied Physics*, Vol. 91, No. 3, 2002, pp. 984–991.

[4]Katz, I., Gardner, B. M., Mandell, M. J., Jongeward, G. A., Patterson, M., and Myers, R. M., "Model of Plasma Contactor Performance," *Journal of Spacecraft and Rockets*, Vol. 34, No. 6, 1997, pp. 824–828.

[5]Polk, J. E., Anderson, J. R., Brophy, J. R., Rawlin, V. K., Patterson, M. J., Sovey, J., and Hamley, J., "An Overview of the Results from an 8200 Hour Wear Test of the NSTAR Ion Thruster," AIAA Paper 99-2446, June 1999.

[6]Malik, A. K., Montarde, P., and Haines, M. G., "Spectroscopic Measurements of Xenon Plasma in a Hollow Cathode," *Journal of Physics D: Applied Physics*, Vol. 33, No. 16, 2000, pp. 2037–2048.

[7]Domonkos, M. T., Gallimore, A. D., Williams, G. J., Patterson, M. J., "Low Current Hollow Cathode Evaluation," AIAA Paper 99-2572, June 1999.

[8]Dettmann, J.-M., and Karstensen, F., "Absolute Ionization Functions for Electron Impact with Barium," *Journal of Physics B: Atomic and Molecular Physics*, Vol. 15, No. 2, 1982, pp. 287–300.

[9]Yagi, S., and Nagata, T., "Absolute Total and Partial Cross-Sections for Ionization of Ba and Eu Atoms by Electron Impact," *Journal of the Physical Society of Japan*, Vol. 69, No. 5, 2000, pp. 1374–1383.

[10]Koveleski, S. D., "Life Model of Hollow Cathodes Using a Barium Calcium Aluminate Impregnated Tungsten Emitter," International Electric Propulsion Conf. IEPC Paper 01-276, Oct. 2001.

[11]Sovey, J. S., Hamley, J. A., Haag, T. W., Patterson, M. J., Pencil, E. J., Peterson, T. T., Pinero, L. R., Power, J. L., Rawlin, V. K., Sarmiento, C. J., Anderson, J. R., Becker, R. A., Brophy, J. R., Polk, J. E., Benson, G., Bond, T. A., Cardwell, G. I., Christensen, J. A., Frieck, K. J., Hamel, D. J., Hart, S. L., McDowell J., Norenberg, K. A., Phelps, T. K., Solis, E., Yost, H., and Matranga, M., "Development of an Ion Thruster and Power Processor for New Millennium's Deep Space 1 Mission," AIAA Paper 97-2778, July 1997.

[12]Reid, R. C., Prausnitz, J. M., and Sherwood, T. K., *The Properties of Gases and Liquids*, 3rd ed., McGraw–Hill, New York, 1977, pp. 402, 403.

[13]Williams, G. J., Jr., "The Use of Laser-Induced Fluorescence to Characterize Discharge Cathode Erosion in a 30 cm Ring-Cusp Ion Thruster," Ph.D. Dissertation, Dept. of Aerospace Engineering, Univ. of Michigan, Ann Arbor, MI, Dec. 2000, p. 78.

[14]Book, D. L., *NRL Plasma Formulary*, Naval Research Lab., Washington, DC, 1987, pp. 33–34, 38.

[15]Mikellides, I. G., Katz, I., Mandell, M. J., and Snyder, J. S., "A 1-D Model of the Hall-Effect Thruster with an Exhaust Region," AIAA Paper 2001-3505, July 2001.

[16]Siegfried, D. E., and Wilbur, P. J., "An Investigation of Mercury Hollow Cathode Phenomena," AIAA Paper 78-705, April 1978.

[17]Lister, G. G., Curry, J. J., and Lawler, J. E., "Modeling of Low-Pressure Barium-Rare-Gas Discharges," *Physical Review E: Statistical Physics, Plasmas, Fluids, and Related Interdisciplinary Topics*, Vol. 62, No. 4, 2000, pp. 5576–5583.

[18]Palluel, P., and Shroff, A. M., "Experimental Study of Impregnated-Cathode Behavior, Emission, and Life," *Journal of Applied Physics*, Vol. 51, No. 5, 1980, pp. 2894–2902.

[19]Rawlin, V. K., Sovey, J. S., Anderson, J. R., Polk, J. E., "NSTAR Flight Thruster Qualification Testing," AIAA Paper 98-3936, July 1998.